 Bull. Chem. Soc. Jpn., 75, 1269–1273 (2002)

Electrochemical and In Situ SNIFTIR Spectroscopic Studies of Palladium(II) and Zinc(II) Schiff Base Complexes: Structural Control of the Electronic Communication between Two Identical Redox Sites

Xiayan Wang, Zhaoxiang Deng,[†] Baokang Jin,[*,††] Yupeng Tian,[††,#] Xiangqin Lin[*]

Department of Chemistry, University of Science and Technology of China, Hefei 230026, China

[†]Department of Chemistry, Inorganic Institute, Tsinghua University, Beijing 100084, China

[††]Department of Chemistry, Anhui University, Hefei 230039, China

(Received November 13, 2001)

The mechanisms of the electron transfer of *S*-benzyl-*N*-(ferrocenyl-1-methyl-methylidene)-dithiocarbazate palladium(II)/zinc(II) complexes $[Pd(lsb)_2]$/$[Zn(lsb)_2]$ were studied by cyclic voltammetry, differential pulse voltammetry, digital simulation and in-situ subtractively normalized interfacial Fourier transform infrared (SNIFTIR) spectroelectrochemistry. The results indicate that $[Pd(lsb)_2]$, which has a square-planar configuration, involved two consecutive one-electron steps in the redox process, while the tetrahedral configuration of Zn(II) involved a two-electron step. The $[Pd(lsb)_2]$ complex exhibits a moderately strong electronic communication between the two-ferrocene moieties, which occurs through the skeleton chain of the ligand due to extensive electron delocalization of the whole molecule during the redox process, while the $[Zn(lsb)_2]$ complex shows low electron delocalization, and has two almost identical ferrocene moieties.

There is a current interest in the synthesis of new materials with large optical nonlinearities, and organometallic compounds have been shown to be a useful general class of such materials.[1–9] Compared to common organic molecules, they offer a larger variety of novel structures, possibility of high environmental stability, and diversity of tunable electronic behavior by virtue of coordinated metal centers, which might result in nonlinear optical (NLO) materials with unique characteristics, such as magnetic and electrochemical properties.[10] Ferrocene, owing to its unique and valuable redox and photophysical properties, has been widely used in constructing molecular systems containing multiple redoxative centers.[11–12] Metal-bridged biferrocene complexes are one kind of the most efficient third-order nonlinear optical organometallic compounds.[13]

Because the properties of biferrocenes depend upon the amount of delocalization or the extent of interaction between the two or more moieties, the nature and extent of electronic intramolecular communication between two or more identical redox centers has received considerable attention.[14] In the present work, electrochemical measurements, digital simulations and in situ SNIFTIR were combined to study the mechanism of electron transfer of metal-bridged biferrocene trinuclear complexes, $[Pd(lsb)_2]$/$[Zn(lsb)_2]$, derived from a Schiff-base ligand, Hlsb, *S*-benzyl-*N*-(ferrocenyl-1-methyl-methylidene)-dithiocarbazate, during a redox process.

State Key Laboratory of Coordination Chemistry, Nanjing University, Nanjing 210093, China

Experimental

Preparation of the Ligand (Hlsb). *S*-benzyl dithiocarbazate was synthedized according to a previously reported method.[15] After two drops of acetic acid were added to a mixture of *S*-benzyldithiocarbazate and acetylferrocene in refluxing ethanol, upon cooling a red-brown solid was formed. The solid was collected by filtration and washed with ethanol and dried in a vacuum.

Preparation of $[Pd(lsb)_2]$ and $[Zn(lsb)_2]$. An ethanol solution of the ligand and $[PdCl_2(CH_3CN)_2]$ or $Zn(OAc)_2{\cdot}nH_2O$ were mixed. A brown or red-brown crystalline solid, which formed after refluxing for 4h, was collected by filtration, washed with ethanol and dried in a vacuum. The molecular structures of the two complexes are as shown in Scheme 1.

The details of the design, synthesis, structural characterization and NLO properties will be reported elsewhere.[15]

Electrochemical Measurements. Electrochemical measurements were conducted on an EG&G PAR Model 283 potentiostat/galvanostat using M270 electrochemical analysis software in a three-electrode cell configuration comprising a BAS glassy carbon (GC) (3 mm in diameter) working electrode, a Ag/AgCl reference electrode and a coiled platinum wire counter electrode. Cyclic voltammograms were obtained in a CH_2Cl_2 solution containing 0.1 M tetrabutylammonium perchlorate (TBAP) as a supporting electrolyte.

In Situ SNIFTIR Spectroscopic Measurements. Subtractively normalized interfacial Fourier transform infrared (SNIFTIR) spectroscopic measurements were performed by an in-situ method on a Nicolet Nexus 870 spectrometer equipped with a variable-angle specular-reflectance accessory (VeeMax II) and a HgCdTe/A (MCT/A) detector cooled with liquid nitrogen.

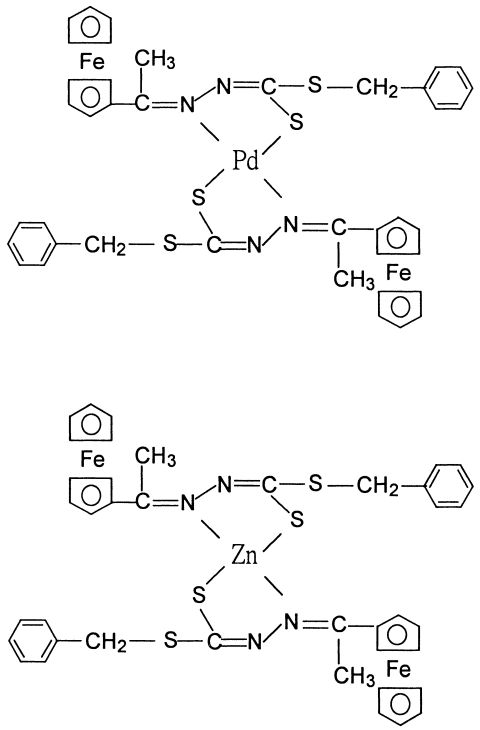

Scheme 1.

A syringe-type in situ reflection–absorption spectroelectrochemical cell was made from Teflon. A platinum wire and a silver wire were fixed in the cell body used as a counter electrode and a reference electrode, respectively. A disk of sodium chloride was used as an IR transparent window. The working electrode was a BAS GC disk, which was first polished with an aqueous suspension of 0.1 μm alumina to obtain a mirrorlike surface, and then washed with doubly distilled water in an ultrasonic bath. While measuring the in situ SNIFTIR spectra, the working electrode was pushed against the window to form a thin electrolyte layer in the spectroelectrochemical cell. The incident angle was adjusted to 60°. A total of 50 interferometric scans with a resolution of 4 cm^{-1} were accumulated for an averaged spectrum. The spectra were successively taken while the electrode potential was scanned at a rate of 2 mV s^{-1}. The resulting spectra were normalized as

$$\Delta R/R = [R(E_S) - R(E_R)]/R(E_R).$$

By subtracting the reflection spectrum at the sample potential (E_S, $R(E_S)$), from the reflection spectrum at reference potential (E_R, $R(E_R)$), the background due to the absorption of the solvent system was eliminated.

Results and Discussion

Electrochemical Results. Cyclic voltammograms for Hlsb, $[Zn(lsb)_2]$ and $[Pd(lsb)_2]$ at a glassy carbon electrode in a CH_2Cl_2 solution containing 0.1 M TBAP were studied. As illustrated in Fig. 1, the voltammogram of Hlsb shows a reversible one-electron redox process at $E_{1/2} = 0.608$ V with $\Delta E_p = 0.118$ V at 50 mV s^{-1}. The voltammogram of $[Zn(lsb)_2]$ exhibits a reversible two-electron redox step at $E_{1/2} = 0.685$V with $\Delta E_p = 0.174$ V. This indicates that the two ferrocenyl moiety in $[Zn(lsb)_2]$ are almost identical and that there exits a very

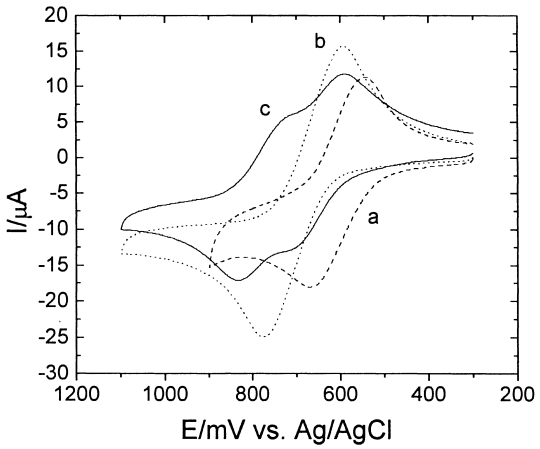

Fig. 1. Cyclic voltammograms of a 1 mM solution of (a) Hlsb, (b) $[Zn(lsb)_2]$ and (c) $[Pd(lsb)_2]$ in 0.1 M TBAP/CH_2Cl_2 at 50 mV s^{-1}.

small interaction between them. From cyclic voltammogram of $[Pd(lsb)_2]$ and $[Zn(lsb)_2]$, it can be seen that the respective redox responses of $[Pd(lsb)_2]$ and $[Zn(lsb)_2]$ are shifted to more positive potentials than those of Hlsb. This indicates that the coordination of the ligand to palladium or zinc makes the electron-withdrawing ability of the dithiocarbazate group somewhat stronger. The voltammetric behavior of $[Pd(lsb)_2]$ appears to involve two diffusion-controlled, reversible redox processes; also, because the corresponding two half-wave potentials are close, the two voltammetric waves are not fully resolved. The determination of the number of electrons transferred in the complete oxidation of $[Pd(lsb)_2]$ was effected by exhaustive coulometry measurements, carried out past the anodic wave at a higher potential ($E = 1.10$ V), resulting in the removal of 2 electrons/molecule. The two consecutive one-electron oxidation steps presumably give the corresponding mono- and then di-ferrocenium cations[16] (Eq. 1) (where Fc = ferrocenyl):

$$\underset{\mathbf{1}}{\text{Fc–Pd unit–Fc}} \underset{+e}{\overset{-e^-}{\rightleftharpoons}} \underset{\mathbf{1}^+}{(\text{Fc–Pd unit–Fc})^+} \underset{+e}{\overset{-e^-}{\rightleftharpoons}} \underset{\mathbf{1}^{2+}}{(\text{Fc–Pd unit–Fc})^{2+}} \quad (1)$$

The results also show that it is appreciably more difficult to remove the second electron than the first one, thus indicating an electronic interaction between the ferrocene and ferroenium units in the mono-cation. Two types of interactions may be envisaged, operating either through the carbon skeleton of the ligand[17] or via a direct metal-metal interaction or field effect.[18]

A differential pulse voltammogram (DPV) of $[Pd(lsb)_2]$ in a dichloromethane solution is shown in Fig. 2. It shows two sufficiently well separated peaks of equal height. The half-wave potentials were calculated from the DPV peak potentials,

$$E_{1/2} = E_p + E_d/2,$$

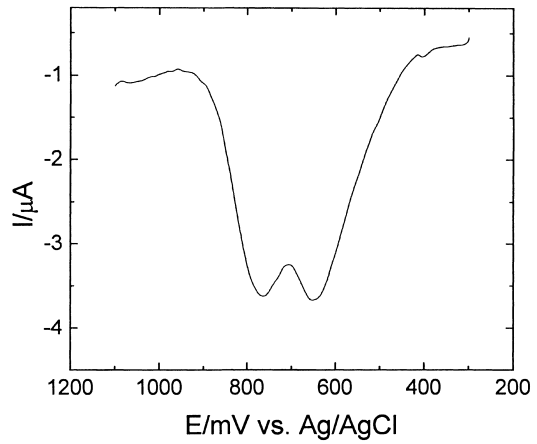

Fig. 2. Differential pulse voltammogram of 1 mM $[Pd(lsb)_2]$ in 0.1 M TBAP/CH_2Cl_2 at 10 mV s^{-1} with pulse height of 10 mV.

where E_p and E_d and the peak potential and the pulse height, respectively.

The obtained results were ${}^1E_{1/2} = 0.657$ V for the process corresponding to the first peak and ${}^2E_{1/2} = 0.769$ V for the second. The corresponding $\Delta E_{1/2}$ value of 112 mV reveals a moderately strong level of electronic communication between the two ferrocene residues.[19]

Digital Simulation. The experimental voltammogram of $[Pd(lsb)_2]$ in Fig. 1 is characteristic of an EE electron-transfer process. A digital simulation was employed to obtain the corresponding redox half-wave potentials. All of the simulations were carried out using a home-built electrochemical simulator package, which is capable of simulating virtually any user-defined electrochemical mechanism. The simulator is realized based on an exponentially expanding grid network approach[20,21] employing a spatial finite-difference discretization of the governing reaction–diffusion equations and a gear-trapezoidal temporal integration scheme. The electrochemical process subject to the simulations could be denoted as follows:

$$(1)\ \mathbf{1} - e \rightarrow \mathbf{1}^+,$$

$$(2)\ \mathbf{1}^+ - e \rightarrow \mathbf{1}^{2+},$$

$$(3)\ \mathbf{1} + \mathbf{1}^{2+} = 2\mathbf{1}^+.$$

Reaction (3) is usually called a comproportionation reaction, the equilibrium constant of which is dependent on the difference of the two formal potentials for reaction (1) and (2) in the following way:

$$K_C = \exp(\Delta E^\circ F/RT),$$

where F is the Faraday constant, R is the gas constant and T is the thermodynamic temperature. During the simulation, the rates of reactions (1) and (2) were assumed to be fast enough to satisfy Nernstian electron-transfer approximations. Reaction (3) was assumed to be a fast equilibrium process with extremely large rate constants for both the forward and backward reactions, so that equilibrium could always be maintained during the voltammeric measurements. Fitting the experimental voltammogram to digital simulations (Fig. 3(a)) yielded 0.642 and 0.762 V for the two $E_{1/2}$ values, corresponding to a $\Delta E_{1/2}$ of 120 mV and an equilibrium constant (K_C) of 107 (assuming the diffusion coefficients for species $\mathbf{1}$, $\mathbf{1}^+$ and $\mathbf{1}^{2+}$ to be equal) for the comproportionation solution electron-transfer (SET) reaction (reaction 3). This value of $\Delta E_{1/2}$ coincides with the result obtained from DPV, and reveals a moderately strong electronic interaction between the two redox-active sites in $[Pd(lsb)_2]$, compared with the statistically derived $\Delta E_{1/2}$ of 36 mV for identical, non-interacting metal ions in homobinuclear complexes. It is noteworthy that the influence of the uncompensated solution resistance ($R_u = 2000\ \Omega$) and the double-layer ca-

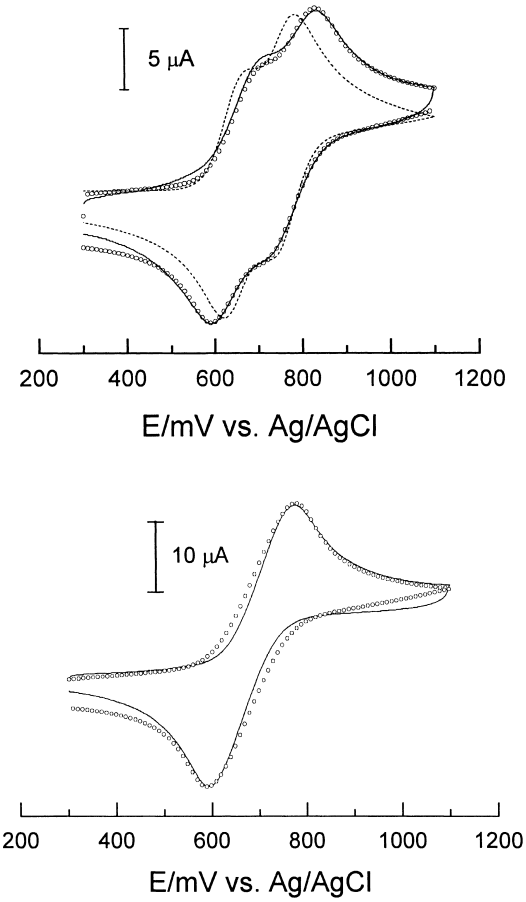

Fig. 3. (a) Experimental and simulated cyclic voltammograms for $[Pd(lsb)_2]$. Solid line, experimental curve; circles, simulated voltammetric curve considering the distortion by R_u and C_{dl}; dotted line, simulated voltammogram without considering R_u and C_{dl}. Parameters used in the simulation are $\nu = 50$ mV s^{-1}, $E_{1/2} = 0.642$ and 0.762 V for the first and second voltammetric waves respectively, $K_c = 107$, ${k^0}_1 = {k^0}_2 = 1$ cm s^{-1}, $R_u = 2000\ \Omega$, $C_{dl} = 20\times10^{-6}$ F. (b) Experimental and simulated cyclic voltammograms for $Zn(lsb)_2$. Solid line, experimental voltammogram; open circles, simulated voltammetric curve considering the distortion by R_u. Parameters used in the simulation are $\nu = 50$ mV s^{-1}, $E_{1/2} = 0.650$ and 0.686 V for the two consecutive redox processes respectively. ${k^0}_1 = {k^0}_2 = 1$ cm s^{-1}, $R_u = 2400\ \Omega$.

pacitance ($C_{dl} = 20\times10^{-6}$ F) on the resulting current response had to be considered during the simulations to account for the apparent deviation of the voltammetric curve from the Nernstian type; otherwise, no acceptable fitting could be obtained. As a contrast, the simulated voltammogram without considering the influence of R_u and C_{dl} is also provided as shown in Fig. 3(a) (dotted line), which shows sharper voltammetric peaks and much smaller peak separations. Fig. 3(b) shows the experimental and simulated cyclic voltammograms for $Zn(lsb)_2$. Fitting of the experimental voltammogram to digital simulations yielded 0.650 and 0.686 V for the two $E_{1/2}$ values, corresponding to $\Delta E_{1/2} \approx 36$ mV, which indicates that there is a very small interaction between the two redox sites.

In Situ SNIFTIR Spectroscopy. The SNIFTIR spectra of $[Zn(lsb)_2]$ and $[Pd(lsb)_2]$ recorded during the oxidation processes in the spectral range of 1700–1300 cm^{-1} are shown in Figs. 4 and 5. In measuring of the SNIFTIR spectra, E_R was set at +0.20 V, where no redox reaction of the two complexes occurred. In the subtractively normalized spectra, the upward peak indicates the disappearance of a certain group, while downward indicates its appearance.

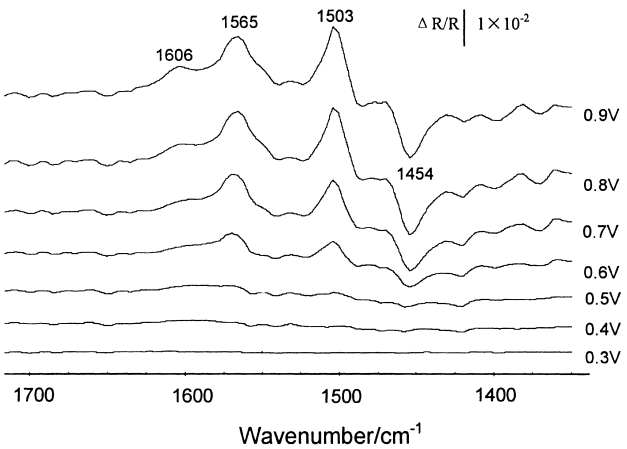

Fig. 4. In situ SNIFTIR spectra of 5 mM $[Pd(lsb)_2]$ in 0.1 M TBAP/CH_2Cl_2, Potential scan rate: 2 mV s^{-1}. E_R = +0.2 V vs Ag/AgCl.

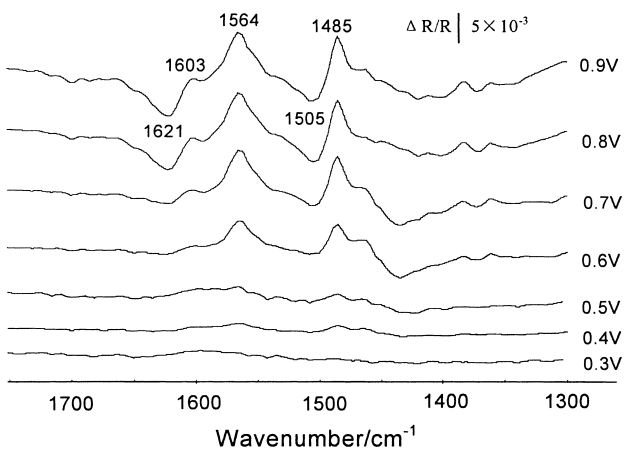

Fig. 5. In situ SNIFTIR spectra of 5 mM $[Zn(lsb)_2]$ in 0.1 M TBAP/CH_2Cl_2. Potential scan rate: 2 mV s^{-1}. E_R = +0.2 V vs Ag/AgCl.

From Fig. 4, it can be seen that two distinct upward peaks appeared at 1565 cm^{-1} and 1503 cm^{-1} which can be ascribed to the $\nu_{C=N}$ stretching modes.[22] These peaks appear from +0.6 V, indicating the beginning of $[Pd(lsb)_2]$ oxidation at this potential; also, the peak intensities increased with the increasing of the electrode potential. It is clear that the characteristic of the C=N double bond is reduced during the oxidation process. This is because oxidation of the ferrocene unit inductively decreases the electron density on the C=N group attached to the cyclopentadienyl ring, resulting in a loss of strength in the C=N bond.

The structure of $[Pd(lsb)_2]$[15] shows that the Pd(II) atom is coordinated in a slightly distorted square-planar configuration with two equivalent Pd–N bonds and Pd–S bonds. The dihedral angle between the two coordination planes is 12.1°. Two cyclopentadienyl units and the Pd(II) moiety are almost in a planar configuration, and forms a larger π-conjugation system favorable for electron transfer through the ligands. The iron-iron distance is 7.314 Å in $[Pd(lsb)_2]$, which is relatively long so as to minimize the interaction between the iron atoms. The iron-palladium distance is 4.982 Å in $[Pd(lsb)_2]$. Delocalization of the Pd electron density into the spacer chain through a $d\pi \rightarrow p\pi$ interaction is present.[23] The Pd(II) moiety is available to form a large π-conjugation system with cyclopentadienyls, which facilitates the transfer an electron through the ligand.

Because the molecular orbitals of the ferrocenyl group consist of HOMO and LUMO of an iron atom and a ligand, there is possibly a cooprative bonding action within Fe–C_5H_5. The ligand offers electron density to the iron atom, whereas the iron atom feeds back the electron density to the ligand simultaneously. The net result of the two contrast actions is that the electron density is transferred from the ligand to the iron atom due to the weak π acid of the ligand.[24] The iron atoms lose electrons in the oxidation of $[Pd(lsb)_2]$, resulting in the donor strength of $C_5H_5 \rightarrow$ Fe being increased and the π-bonding electron density being decreased within the ligand molecule. Thus, the new strong downward band at 1454 cm^{-1} is assigned to $\nu_{C=C}$ stretching vibration.[25] The formation of this band may be due to a change of cyclopentadienyl resulting from extensive electron delocalization of the whole molecule. Thus, electron transfer through the ligand is dominant in the $[Pd(lsb)_2]$ complex, and can be represented schematically in Scheme 2.

Figure 5 is the spectra of $[Zn(lsb)_2]$, and is obviously different from those of $[Pd(lsb)_2]$. From 0.6 V, two obvious positive peaks appear at 1564 cm^{-1} and 1485 cm^{-1}, and two negative peaks at 1621 cm^{-1} and 1505 cm^{-1}. The peaks at 1564 cm^{-1} and 1485 cm^{-1} can be assigned to the $\nu_{C=N}$ stretching modes of $[Zn(lsb)_2]$[22]. Because the two peaks shift to higher wavenumbers along with an increase in the electrode potential, the bands at 1621 cm^{-1} and 1505 cm^{-1} can be attributed to the $\nu_{C=N}$ stretching modes of $[Zn(lsb)_2]^{2+}$. An upward peak near 1600 cm^{-1} is observed in both Figs. 4 and 5, which maybe assigned to the $\nu_{C=C}$ stretching mode of phenyl. The certain contribution of this band needs further study.

The structure of $[Zn(lsb)_2]$[15] shows that the Zn(II) atom is coordinated in the tetrahedral configuration. The dihedral angle between the two coordination planes is 63.2°. The iron-

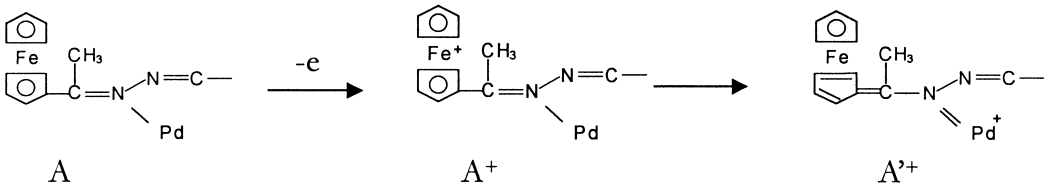

Scheme 2.

iron distance is 7.606 Å in $[Zn(lsb)_2]$, which is relatively long to minimize the interaction between the iron atoms, and the iron-zinc distance is 5.051 Å. The large space block resulting from the tetrahedral configuration of $[Zn(lsb)_2]$ makes the Zn(II) atom difficult to form a large π-conjugation system, which brings on a low degree electron delocalization and obstructs the electron transfer carryied out through the ligand. There is therefore a slight electronic communication between the two redox sites. This is the reason that the band at 1454 cm^{-1} doesn't appear in Fig. 5, but appears in Fig. 4.

Conclusion

In this paper, two novel biferrocene trinuclear complexes, $[Pd(lsb)_2]$ and $[Zn(lsb)_2]$, derived from the Schiff-base ligand, Hlsb, *S*-benzyl-*N*-(ferrocenyl-1-methyl)-dithiocarbazate, were characterized by cyclic voltammetry, differential pulse voltammetry, a digital simulation, and in-situ SNIFTIR spectroscopy. The tetrahedral configuration complex, $[Zn(lsb)_2]$, involved one two-electron redox process. The two redox sites are almost identical in the molecule, and there is a slight electronic communication between them. The space block hinders electron transfer between the two ferrocene. The square-planar configuration complex, $[Pd(lsb)_2]$, shows two consecutive one-electron steps to give corresponding mono- and then diferrocenium cations in the potential region between 0.3 V and 1.0 V vs Ag/AgCl. This complex exhibits a moderately strong degree of electronic communication between the two-ferrocene moieties. In situ SNIFTIR results indicate that the electron transfer of $[Pd(lsb)_2]$ takes place through the skeleton chain of the ligand due to extensive electron delocalization of the whole molecule during the redox processes.

This work was supported by the National Natural Science Foundation of China (No. 20071001).

References

1 M. L. H. Green, S. R. Marder, M. E. Thompson, J. A. Bandy, D. Bloor, P. V. Kolinsky, and R. J. Jones, *Nature*, **330**, 360 (1987).

2 S. R. Marder, J. W. Perry, B. G. Tiemann, and W. P. Schaefer, *Organometallics*, **10**, 1991 (1896).

3 N. J. Long, *Angew. Chem., Int. Ed. Engl.*, **34**, 21 (1995).

4 D. R. Kanis, M. A. Ratner, and T. J. Marks, *J. Am. Chem. Soc.*, **112**, 8203 (1990).

5 M. E. Wright and E. G. Toplilar, *Macromolecules*, **25**, 1838 (1992).

6 J. Zyss, "Molecular Nonlinear Optics," Academic Press, New York (1994).

7 D. M. Burland, *Chem. Rev.*, **94**, 1 (1994).

8 S. R. Marder and D. N. Beratan, and L. T. Cheng, *Science*, **252**, 103 (1991).

9 H. K. Sharma, K. H. Pannell, I. Lecloux, J. Zyss, A. Ceccanti, and P. Zanello, *Organometallics*, **19**, 770 (2000).

10 G. G. A. Balavoine, J. C. Daran, G. Iftime, P. G. Lacroix, E. Manoury, J. A. Delaire, I. M. Fanton, K. Nakatani, and S. D. Bella, *Organometallics*, **18**, 21 (1999).

11 K. W. Poon, Y. Yan, X. Y. Li, and D. K. P. Ng, *Organometallics*, **18**, 3528 (1999).

12 B. Bildstein, M. Malaun, H. Kopacka, K. Wurst, M. Mitterbock, K. H. Ongania, G. Opromolla, and P. Zanello, *Organometallics*, **18**, 4325 (1999).

13 Y. P. Tian, Z. L. Lu and X. Z. You, *Acta Chim. Sin.*, **57**, 1068 (1999).

14 J. Alvarez and A. E. Kaifer, *Organometallics*, **18**, 5733 (1999).

15 Y. P. Tian, in preparation.

16 J. E. Gorton, H. L. Lentzner, and W. E. Watts, *Tetrahedron*, **27**, 4353 (1971).

17 D. W. Hall, E. A. Hill, and J. H. Richards, *J. Am. Chem. Soc.*, **90**, 4972 (1968).

18 H. L. Lentzner and W. E. Watts, J. Chem. Soc., *Chem. Commun.*, **1970**, 906.

19 J. B. Flannagan, S. Margel, A. J. Bard, and F. C. Anson, *J. Am. Chem. Soc.*, **100**, 4248 (1978).

20 J. Horno and M. T. García-Hernández, *J. Electroanal. Chem.*, **352**, 83 (1993).

21 Z. X. Deng and X. Q. Lin, Fenxi Huaxue, (*Chinese J. Anal. Chem.*), **27**, 1376 (1999).

22 C. Y. Duan, Y. P. Tian, Z. H. Liu, X. Z. You, and T. C. W. Mak, *J. Organomet. Chem.*, **570**, 155 (1998).

23 K. R. J. Thomas, J. T. Jiann, and K. J. Lin, *Organometallics*, **18**, 5285 (1999).

24 "Fundamental Transmit element organometallic chemistry," ed by Charles M. Lukehart, and, trans. by Q. Z. Shi, Y. C. Gao and X. Q. Xue, Lanzhou University Press, Lanzhou (1989), Ch. 4.

25 L. J. Bellamy, "The Infrared Spectra of Complex Molecules," London, Chapman and Hall (1975).